

Galaxy cluster A2142: halo boundary, „red sequence“, properties of galaxies according to SDSS

F.G. Kopylova,¹ and A.I. Kopylov¹

¹*Special Astrophysical Observatory of the Russian AS, Nizhnij Arkhyz 369167, Russia*

The paper presents the results of studying the dynamics of galaxies, properties of early-type galaxies, properties of galaxies with the quenched star formation (QGs) in the A 2142 based on the archival data from the Sloan Digital Sky Survey. We found the observed halo boundary, the splashback radius R_{sp} , which is equal to 4.12 Mpc ($M_r < -20^m3$) and 4.06 Mpc ($M_r < -21^m5$) over the integral distribution of the number of galaxies as a function of the squared distance from the center. We have studied how early-type galaxies are distributed in the center and in the outskirts of the cluster ($R/R_{200} < 3$, $M_r < -20^m3$) and plotted the red sequence in the form of $(g - r) = (-0.024 \pm 0.001)M_r + (0.441 \pm 0.005)$. Among all the cluster galaxies, the galaxies with the quenched star formation ($-12 \text{ yr}^{-1} < \log sSFR < -10.75 \text{ yr}^{-1}$) make up about one third. We have found that the fraction of QGs beyond the splashback R_{sp} is the same as in the field at the same z with coordinates of the center of 16^h5 , 31° and a size of $300'$. For galaxies with the stellar masses $\log M_*/M_\odot = [10.5; 11.0]$ (this is the main mass range of QGs), after entering the cluster, there is a decrease in the radii $R_{90,r}$ by about 30% when moving towards the center.

Keywords: galaxies: clusters: individual: A 2142 — galaxies: star formation - galaxies: evolution

1. INTRODUCTION

Galaxy clusters, the largest gravitationally bound systems in the Universe, are the main objects of the observational cosmology [1] allowing one to study the hierarchical growth of structures. For such studies, one of the best targets in the local Universe ($z < 0.1$) is the cluster A 2142 with the highest luminosity in the X-ray and with a large number of galaxy groups in its outskirts, which it gravitates. When observing the cluster in the X-ray (Chandra, XMM-Newton), multiple concentric cold fronts of surface brightness [2, 3] were found indicating the sloshing activity of the core [4, 5] stretching up to 1 Mpc from the center of the cluster [3]. A two-component radio halo [6] was detected in the radio range (observations with LOFAR and VLA). Eckert et al. (2014) also found

evidence of accretion of gas and galaxies onto the cluster: the galaxy group was discovered at a distance of 1.5 Mpc northeast of the main system.

The central region of the A2142 has been studied in the optical range. Owers et al. (2011) identified several subclusters falling on it in the distribution of galaxies near the cluster (up to 2 Mpc). Einasto et al.(2020) have shown that the cluster A2142 is the result of past and present galaxy mergers. Liu et al. (2018) found 19 subclusters within 3.5 Mpc and studied multiple mergers of smaller subsystems with the main cluster, which influenced its complex dynamics. In addition, in the indicated paper, the gas rings were found near two cold fronts seen in the X-ray region. The velocities of the rings exceed the average radial velocity of the cluster by 810 ± 330 and 660 ± 300 km s⁻¹. Liu et al.(2018) explained these features of the gas in terms of a core sloshing activity model.

The objectives of this paper are to determine the boundary of the A 2142 and the characteristics of its constituent galaxies: the fraction of early-type galaxies in the red sequence and galaxies with the quenched star formation along the normalized radius, as well as to reveal changes in the radius $R_{90,r}$ of the galaxies along the radius of the cluster.

We carried out the study using the data from the SDSS catalog (Sloan Digital Sky Survey Data Release 7 [11], 10 [12]), and NED (NASA Extragalactic Database). The paper is organized as follows. Section 2 describes the procedure of measuring the dynamical characteristics of the galaxy cluster and determining its surroundings. Section 3.1 presents the plotted color-magnitude relation of early-type galaxies, estimates of the fraction of early-type galaxies along the radius and their characteristics at a fixed stellar mass, and compares this fraction with the values obtained for field objects. In Section 3.2, the specific star formation rate of galaxies is considered; galaxies with the quenched star formation (QGs) are found. The fraction of QGs along the radius is determined at a fixed stellar mass of galaxies, their characteristics are given, and a comparison is made with the specific star-formation rate in the field. Section 4 lists the main results. In the paper, we used the following cosmological parameters: $\Omega_m = 0.3$, $\Omega_\Lambda = 0.7$ and $H_0 = 70$ km s⁻¹ Mpc⁻¹.

2. DYNAMICAL CHARACTERISTICS

The completeness of the galaxy cluster under study is determined by the completeness of the spectroscopic data of the SDSS catalog. Strauss et al. (2002) applied the following conditions when selecting the galaxies (the Main galaxy sample): $r_{\text{Pet}} < 17.^m77$ and $\langle \mu_r \rangle < 24.^m5$, where r_{Pet} is the Petrosian magnitude of the galaxy in the r filter corrected for extinction in the Galaxy, and

$\langle\mu_r\rangle$ is the Petrosian average surface brightness corresponding to the effective radius. Under these conditions, the completeness of the SDSS galaxies was 99% and for bright galaxies 95%.

Usually, when studying galaxy clusters, to increase the spectral completeness of bright galaxies in the absence of the SDSS measurements of their radial velocities, we added the data from the NED database. If there were no such measurements in the NED, we selected early-type bright red sequence galaxies as probable cluster members (from one to five galaxies) using the color-magnitude diagrams $((u-r), M_r; (g-r), M_r; \text{ and } (r-i), M_r)$ [14, 15].

Determination of the dynamical characteristics of the system of galaxies: the radial velocity, the dispersion of the radial velocities and mass is performed for a region of the radius R_{200c} . The radius R_{200c} (hereinafter R_{200}) is the empirical radius, within which the density in the system 200 times exceeds the critical density of the Universe and can be estimated by the formula: $R_{200} = \sqrt{3}\sigma / (10H(z))$ Mpc [16]. Then, assuming that the cluster is virialized within this radius, $M_{200} \sim M_{\text{vir}}$, we find the mass $M_{200} = 3G^{-1}R_{200}\sigma_{200}^2$. That is, the mass of the cluster measured by us $M_{200} \propto \sigma^3$. The mass M_{200} enclosed in a region of the radius R_{200} can be determined directly from the critical density which depends on z :

$$M_{200} = \frac{4}{3}\pi R_{200}^3 \times 200\rho_c.$$

In model calculations, the radius R_{200m} is often used; this is the radius, within which the density in the system 200 times exceeds the average density of the Universe. We present the main cluster parameters for the region with the radius R_{200} (according to the SDSS DR7 data): the radial velocity dispersion of galaxies, the radii (R_c , R_{200} , and R_{sp}), the heliocentric redshift, the dynamical mass, and the X-ray luminosity in the paper by Kopylova and Kopylov (2015) with the corresponding references and in the columns of Table 1. Our estimates of R_{200} and M_{200} for the cluster are in good agreement with the data from the paper by [18] which collects the results of determining these parameters by the methods different from ours.

The structure and kinematics of A 2142, as well as its immediate surroundings, can be characterized in more detail using the panels of Fig. 1: (a) the deviation of the radial velocities of galaxies—the cluster members and background galaxies—from the average radial velocity depending on the square of the distance from the cluster center; (b) the location of galaxies in the sky plane in equatorial coordinates; (c) the integral distribution of the number of galaxies depending on the square of the distance from the center; (d) the histogram of the distribution of radial velocities of all the galaxies within the radius R_{200} . Note (see Fig. 1a) that the cluster is located along the line

of sight, except for a group of galaxies with $cz < 2500 \text{ km s}^{-1}$ at the bottom of the panel. Figure 1b shows the cluster profile in the projection (the integral distribution of the number of galaxies depending on the squared radius from the center). It shows that the cluster first has a steep increase in the number of galaxies, and then the number of galaxies located outside the virialized region grows linearly (the straight line in the figure). In our paper [19], a cluster halo-bounding radius R_h was defined, which we later identified with the splashback radius. On closer examination, it turned out that for massive galaxy clusters of the A 1656 and A 2142 types, it is necessary to use 3-4 radii R_{200} to find the distribution point for the linear section. In the cluster A 2142, the radius $R_{\text{sp}} = 4.12 \text{ Mpc}$ ($M_r < -20^{\text{m}}3$), $R_{\text{sp}}/R_{200\text{c}} = 1.81$ or $R_{\text{sp}}/R_{200\text{m}} = 1.13$. From brighter galaxies with $M_r < -21^{\text{m}}5$, we found $R_{\text{sp}} = 4.06 \text{ Mpc}$. According to the results of the paper (see [20], Fig. 5), the following relationship holds for the A 2142 cluster:

$$\log R_{\text{sp}} = (0.24 \pm 0.03) \log L_X - (7.39 \pm 0.33).$$

The dotted line in Fig. 1 shows the radius of the virialized region R_{200} , the dashed line is the radius of the central region R_c , the dash-dotted line corresponds to the splashback radius R_{sp} and is followed by a steep rise of the number of cluster members replaced by a linear one. Figure 1 below also shows the distribution of bright early-type galaxies (at these z , we estimated the limit M_r for A 2142 approximately equal to $-20^{\text{m}}3$ from which this radius is refined). The observed radius R_{sp} (usually $R_{\text{sp}} > R_{200}$) is the radius of the apocenter of the first orbits of galaxies, to which galaxies fly out of the virialized region after the first passage through the cluster center. That is, the radius R_{sp} separates most galaxies that fall into the cluster for the first time from the collapsing galaxies that are already participating in the virial equilibration. The paper by [21] (Fig. 13) shows the positions of galaxies of all kinds, including those that have escaped from the cluster, in the phase space diagram obtained from model simulations of galaxy clusters.

We measured the radii R_{sp} for a sample of 157 galaxy clusters. They vary in the range from $1.02R_{200}$ to $3.64R_{200}$ depending on the dynamical mass and X-ray luminosity [20] and on average are equal to $1.54R_{200}$.

3. SAMPLES OF GALAXIES AND THEIR PROPERTIES

3.1. Early-type galaxies

It is known that the main population of galaxy clusters at low redshifts ($0 < z < 0.1$) are early-type galaxies which are located mainly in the central virialized regions and are the brightest members. Early-type galaxies follow the color-magnitude relationship called the red sequence (RS). In groups and clusters of galaxies, the RS has a small scatter, since the galaxies are at the same distance. We have found that such galaxies in the virialized regions of galaxy clusters (for example, in the Hercules and Leo superclusters of galaxies) are of the order of 60-70% among galaxies brighter than $M_K = -23^m3$ [22]. Early-type galaxies in this paper are selected according to the following criteria (the r -filter): 1) $fracDeV \geq 0.8$, where the parameter $fracDeV$ (according to the SDSS catalog) characterizes the contribution of the bulge to the galaxy surface-brightness profile; 2) the concentration index $c \geq 2.6$, where $c = r_{90}/r_{50}$ (is equal to the ratio of the radii limiting 90 and 50% of the Petrosian fluxes). In addition, we made the $(u - r)$ color restrictions to exclude spiral galaxies: $\Delta(u - r) \geq -0.2$ which follows from the dependence between the $(u - r)$ color and the absolute magnitude

$$(u - r) = -0.108M_r + 0.63$$

with $2\sigma = 0.2$. One can also make the $(g - r)$ color restrictions to narrow the RS: $\Delta|(g - r)| \geq 0.075$. We took the colors of the galaxies from the SDSS catalog calculated from model magnitudes corrected for the extinction in the Galaxy.

The RS obtained for the A 2142 cluster is shown in Fig. 2a against the background of other galaxies. Figure 2b shows the phase space diagram of the A 2142 in the projection, where $\Delta V/\sigma$ is the ratio of the radial velocity difference of galaxies and the average radial velocity of the cluster to the dispersion of radial velocities, R/R_{200} is the distance of the galaxy from the selected cluster center normalized to the radius R_{200} . We took the brightest galaxy as the center of the system of galaxies, whose coordinates were close to the coordinates of the X-ray center. The solid circles show the RS galaxies within a radius of $3.5R/R_{200}$ (Fig. 2a and Fig. 2b), the open circles mark the rest of the galaxies. The dashed model line [23, 24]) roughly limits the virialized members of the cluster. We took the galaxies with $-2 < \Delta V/\sigma < 2$ as the cluster members beyond the radius R_{200} , therefore, the falling group galaxies (Fig. 1) with Δcz about -2500 km s^{-1} is not shown in the phase diagram.

Some characteristics of early-type galaxies and estimates of their fraction $frac_E$ along the cluster radius are given in Table 2. The first line contains the results for the sample of galaxies on the RS, restricted by the color $\Delta |(g-r)| < 0.075$, as in the papers by [14, 15] (for 40 clusters of galaxies with $z < 0.045$). The second line gives the results without the $(g-r)$ restriction. In total, we found 214 early-type galaxies on the RS in the cluster A 2142 ($R/R_{200} < 3$). If we introduce the color $(g-r)$ restrictions, we get 189 galaxies. It can be noted that the fractions of early-type galaxies on the RS vary along the radius of the A 2142 cluster in the same way as, on average, for nearby galaxy clusters [15]. In order to compare the results obtained for the very rich cluster A 2142 and the results obtained for low-density regions near the cluster, we took a field of a size of $300'$ at the same redshifts ($0.0815 < z < 0.0988$) with the center coordinates ($16^h5, 31^\circ$). With the same selection of early-type galaxies (and taking into account the same condition $M_r < -20^m3$ as for the cluster, we found that the fraction of early-type galaxies in the field is 0.28 ± 0.05 . This is consistent with the values given by Table 2 for the region beyond $R_{sp} = 1.81R_{200}$ or within $2-3 R/R_{200}$. This table also gives the average characteristics of early-type galaxies for the main range of stellar masses $\log M_*/M_\odot = [10.5; 11.0]$. It can be noted that the age of galaxies (in the SDSS DR10, it is defined as the mass-weighted average age of the stellar population in Gyr) slightly decreases, the average effective radius increases by 10%, the average metallicity ($Z_\odot = 0.019$) of the stellar population changes slightly outside the cluster radius R_{200} . It can also be noted that early-type galaxies in the center of the cluster are redder, their effective radius is smaller, they are older and richer in metals than galaxies within a radius of $1-2R_{200}$. The characteristics of galaxies outside the radius R_{sp} differ from the values given for the field. The galaxies in the field are slightly older, richer in metals, and have a smaller radius R_e . The RS plotted from 214 galaxies is described by the expression

$$(g-r) = -0.024(\pm 0.001)M_r + 0.441(\pm 0.005)$$

with $rms = 0.032$. Within error, the shape and zero-point practically do not change with the radius of the cluster.

3.2. Galaxies with the quenched star formation

The so-called „Main Sequence“ relates the star formation rate of spiral galaxies to the stellar mass. As a result of the depletion of gas in galaxies, the star-formation rate falls, and the galaxy moves towards a passive state passing through an intermediate state characterized by the quenched star formation. Within clusters of galaxies, there are different mechanisms that lead to the quenching

of star formation. In the central regions, these are tidal effects, as a result of which galaxies are deprived of gas, stars, and dark matter (e.g., [25]). Some galaxies lose matter, when they are in small groups of galaxies, even before they get into the cluster; that is, they experience pre-processing (e.g., [26–28]).

In Fig. 1b, one can see that the rich cluster A 2142 is surrounded by many groups of galaxies, in which, most likely, pre-processing of galaxies takes place. Earlier, in the paper by [15], for 40 nearby clusters of galaxies ($0.02 < z < 0.045$), we found that even within the radius $2 < R/R_{200} < 3$ (in the outskirts of the considered clusters) the fraction of the galaxies with the quenched star formation is by 27% larger than that in the field.

The specific star formation rate $sSFR$ in the galaxy is defined as the integral star formation rate divided by its stellar mass, $sSFR = SFR/M_*$. The SDSS DR10 catalog contains the results of determining the specific star formation rate, the stellar mass of galaxies, and other parameters galaxies, which have been obtained by fitting the FSPS [29] models to the SDSS photometry in the u , g , r , i , and z filters. We used the model values corrected for extinction and the „early-star formation with dust“ version. In the distribution of galaxies according to the specific star formation rate, $\log sSFR$, a minimum is usually found that separates galaxies with active star formation (active galaxies) from galaxies, in which it is quenched (quenched galaxies–QGs) [30]. In general, the distribution of galaxies in terms of the specific star formation rate $\log sSFR$ has a long tail extending into the region of galaxies without star formation (passive galaxies). In our papers [14, 15], we selected QGs and passive galaxies based on the condition $\log sSFR < -10.75 \text{ yr}^{-1}$. If we exclude galaxies without star formation from the sample ($\log sSFR < -12 \text{ yr}^{-1}$ according to Oemler et al. (2017), there will remain galaxies with the quenched star formation, i.e., those satisfying the condition $-12 \text{ yr}^{-1} < \log sSFR < -10.75 \text{ yr}^{-1}$.

In the studied cluster A 2142 ($R/R_{200} < 3$), we found 188 galaxies with the quenched star formation, 147 of which are early-type galaxies with the parameter $fracDeV \geq 0.8$, the remaining 41 are late-type galaxies. Out of 188 galaxies, 120 have the stellar masses within $\log M_*/M_\odot = [10.5; 11.0]$, 61 galaxies have $\log M_*/M_\odot = [11.0; 11.5]$, and seven more are not included in this range; that is, the galaxies we study are massive ($\log M_*/M_\odot > 10.5$).

Figure 2c shows (with the solid circles) QGs against the background of other galaxies. The first line of Table 3 shows the total fractions of QGs and passive galaxies (similar to those given in the paper by [15], the second line shows only the fractions of QGs along the radius of the A 2142 cluster. It can be noted that the fraction of QGs (including passive ones) is maximum in the central region, somewhat smaller within R_{200} , and drops by about 35% beyond $R_{sp} = 1.81R_{200}$. Beyond

the splashback radius, we have the same number of QGs as in the field 0.58 ± 0.10 (285 galaxies out of 491, $M_r < -20^m3$). At the same time, the fraction of QGs without passive galaxies (the second line of Table 3) is minimum in the center, maximum within the R_{200} radius, and decreases beyond the radius R_{sp} by 28% compared to those in the virialized region of galaxy clusters ($0.1R_{200}$). We have found that the number of such galaxies in the field is approximately the same: 0.31 ± 0.09 , 151 galaxies out of 491 ($M_r < -20^m3$).

Among QGs, the fraction of late-type galaxies identified by the parameter *fracDeV* is insignificant and amounts to 22%. In the center of the $R < 0.25R/R_{200}$ cluster, we found only three. Table 4 shows some properties of late- and early-type QGs in the cluster and in the field at the fixed stellar mass $\log M_*/M_\odot = [10.5; 11.0]$: the stellar population age, metallicity, color ($g - r$), concentration index c , and bulge fraction. The last column of the table shows the parameters of the field galaxies (for 52 late-type galaxies and 48 early-type galaxies). It can be noted that the late-type galaxies falling into the cluster (within R_{200}), become redder, more compact, and similar to early-type galaxies: the concentration index c increases from 2.39 beyond R_{sp} to 2.56, the fraction of the bulge *fracDeV* increases significantly from 0.36 to 0.56 (or by 36%). For early-type galaxies, no significant changes in the parameters are observed. If we compare these parameters of QGs (for the same range of stellar masses) with those from a lower density region (of the field), we can draw the following conclusion. In the cluster region ($R < R_{\text{sp}}$), late-type QGs have a larger bulge, a redder color, and significantly lower metallicity compared to the field galaxies.

In the paper [32], we considered the variations in the stacked Petrosian radius of galaxies in 40 nearby ($0.02 < z < 0.045$) galaxy clusters. For the mass range

$$\log M_*/M_\odot = [10.5; 11.0],$$

it turned out that the radius $R_{90,r}$ of late-type galaxies, when moving inside clusters, decreases by about 13%, and for early-type galaxies—by 11%. In this paper, we also studied the change in the average Petrosian radius $R_{90,r}$ of the galaxies from the A 2142 cluster along its radius for the same range of stellar masses.

Figure 3 shows the change in the average radius $R_{90,r}$ of the galaxies with the quenched star formation, the members of the cluster A 2142, along the normalized radius R/R_{200} . The solid line corresponds to the late-type galaxies (*fracDeV* < 0.8), the dashed line corresponds to the early-type galaxies (*fracDeV* \geq 0.8). The same horizontal lines show the values for field galaxies. We can draw the following conclusions. There are few QGs in the central region of A 2142, but they do

exist. Perhaps, this is the result of a projection of galaxies that do not belong to the cluster. For the galaxies of late and early types that fall into the virialized region of the cluster ($R < R/R_{200}$), the radii $R_{90,r}$ gradually decrease towards the center by approximately 30%. Moreover, one can notice (Fig. 3) that the early-type galaxies have the maximum radius $R_{90,r}$ near the splashback radius, this is not observed for the late-type galaxies. Thus, in the rich cluster A 2142, all the galaxies with the quenched star formation with the mass $\log M_*/M_\odot$ [10.5;11.0] show significant decreases of the radii.

Since the cluster A 2142 is very massive and many groups of galaxies and individual galaxies fall on it even near a radius of $3.5R/R_{200}$ (which can be seen in Fig. 1), the QGs have radii of $R_{90,r}$ somewhat smaller than those in the field, although, within error. Also, we do not detect the effect we found in the paper [32] for nearby clusters of galaxies, when the stacked radii $R_{90,r}$ of the late-type galaxies are maximum near the average stacked splashback radius of clusters. Apparently, the reason is that in A 2142 we deal only with massive galaxies ($M_r < -20^m3$); while in the paper by Kopylova and Kopylov (2020), we studied mostly fainter and less massive galaxies with $M_r > -20^m3$ in nearby clusters. They are 1.5 times greater in number than massive galaxies. That is, the effect we found (although this was not emphasized in the paper by [32]) appears mainly in smaller galaxies, since they are easier to destroy in the field of galaxy clusters. It is known that clustering of galaxies and gas occurs near the radius R_{sp} [35] which results in acceleration of the rate of galaxy changes.

Galaxy clusters can be considered as laboratories, where transformations of galaxies take place. In the papers [33, 34] it is shown that early-type galaxies in clusters are smaller than those in the field. Matharu et al.(2019), for example, found that the increase in the size of passive and star-forming galaxies ($z \sim 1$) in the field compared to those in clusters can be explained by the collision and merging of galaxies. Hamabata et al. (2019) found the radius of the cluster (r is about $0.2h^{-1}$ Mpc, where $h = 0.7$), within which the transformations of spiral galaxies are most effective. The paper by [38] shows how the environment affects spiral galaxies. For a sample, of 700 galaxies ($z < 0.063$, the SDSS data), it was found that sizes of spiral galaxies, in terms of the radius R_e as a parameter, are by 15% smaller in clusters than those in the field, and the *Sersic* parameter is by 15% smaller. Also, the color ($g - r$) of galaxies are redder in clusters.

4. CONCLUSION AND FINDINGS

According to the SDSS data, for the galaxy cluster A 2142 which is the brightest in the X-ray of the local Universe, we have considered the changes: (a) the fraction of early-type galaxies along the radius (in the projection); (b) the fraction of galaxies with the quenched star formation within the nearest outskirts (up to $3R/R_{200}$) in comparison with the data for the field. The paper by [32] showed the changes in the fraction of QGs depending on the stellar mass of galaxies. Massive early-type galaxies tend to be located in the center of the galaxy cluster. The QGs sample that we compiled has stellar masses in the range of $\log M_*/M_\odot = [10.5; 11.5]$ (64% of them are in the range of $\log M_*/M_\odot = [10.5; 11.5]$), that is, these are massive and bright galaxies. We present some properties of these galaxies obtained in that paper.

The key results of this study are the following:

1. From the observed cluster profile—the integral distribution of the number of galaxies depending on the square of the distance from the center—we have found the splashback radius R_{sp} which coincides with the apocenters of the orbits of most galaxies that have already visited the center of the system. The radius R_{sp} of the cluster A 2142 is 4.12 Mpc, $R_{\text{sp}}/R_{200c} = 1.81$ for the critical density, or $R_{\text{sp}}/R_{200m} = 1.13$ for the average density of the Universe.

2. The shape of the color-magnitude (the red sequence, RS) dependence does not change within the considered cluster radius ranges (Table 1). We have obtained the RS as

$$(g - r) = -0.024(-0.023)M_r + 0.441(0.442).$$

The coefficients of the form and zero-point are given for the region with the radius R_{sp} and beyond it (in parentheses). The fraction of early-type galaxies outside R_{sp} is equal to the value for the low-density region, for which the field with the coordinates $16^{\text{h}}5, 31^\circ$ and the radius $300'$ at the same z is taken. The early-type galaxies in the center of the cluster are redder, have a smaller effective radius R_e , are older, and metal-richer than those outside the virial radius, $1-2R_{200}$ (Table 1).

3. The fraction of galaxies with the quenched star formation ($-12 \text{ yr}^{-1} < \log sSFR < -10.75 \text{ yr}^{-1}$) decreases by 28% beyond the radius R_{sp} compared to the radius R_{200} and becomes the same as in the field. Among the QGs, only 22% are late-type galaxies. We have found that in such galaxies both the concentration index and the fraction of the bulge increase towards the center of the cluster, i.e., they become similar to early-type galaxies.

4. It is found that the properties of galaxies with the quenched star formation with the stellar mass $\log M_*/M_\odot = [10.5; 11.0]$, when falling into the rich massive cluster A 2142, change greatly.

The radii $R_{90,r}$ of the galaxies of late and early types decrease by about 30% in the center of the cluster compared to the radii near the boundary of the cluster halo.

ACKNOWLEDGMENTS

This research has made use of the NASA/IPAC Extragalactic Database (NED, <http://nedwww.ipac.caltech.edu>), which is operated by the Jet Propulsion Laboratory, California Institute of Technology, under contract with the National Aeronautics and Space Administration, Sloan Digital Sky Survey (SDSS, <http://www.sdss.org>), which is supported by Alfred P. Sloan Foundation, the participant institutes of the SDSS collaboration, National Science Foundation, and the United States Department of Energy and Two Micron All Sky Survey (2MASS, <http://www.ipac.caltech.edu/2mass/releases/allsky/>).

CONFLICT OF INTEREST

The authors declare no conflict of interest regarding this paper.

References

-
1. A.A. Vikhlinin, A.V. Kravtsov, M.L. Markevitch et al., *Physics-Uspekhi* **57**, 4 (2014).
 2. M. Markevitch, T.J. Ponman, P.E.J. Nulsen et al., *Astrophys. J.* **541**, 542 (2000).
 3. M. Rossetti, D. Eckert, S. De Grandi et al., *Astronom. and Astrophys.* **556**, A4 (2013).
 4. E.R. Tittley, & M. Henriksen, *Astrophys. J.* **618**, 227 (2005).
 5. M. Markevitch, & A. Vikhlinin, *Phys. Rep.* **441**, 1 (2007).
 6. T. Venturi, M. Rossetti, G. Brunetti et al., *Astronom. and Astrophys.* **603**, A125 (2017).
 7. D. Eckert, S. Molendi, M. Owers, et al., *Astronom. and Astrophys.* **570**, A119 (2014).
 8. M.S. Owers, P.E.J. Nulsen, & W.J. Couch, *Astrophys. J.* **741**, 122 (2011).
 9. M. Einasto, B. Deshev, H. Lietzen et al., *Astronom. and Astrophys.* **641**, A172 (2020).
 10. A. Liu, H. Yu, A. Diaferio et al., *Astrophys. J.* **863**, 102 (2018).
 11. K.N. Abazajian, J.K. Adelman-McCarthy, M.A. Aqü eros et al., *Astrophys. J. Suppl.* **182**, 543 (2009).
 12. H. Aihara, C. Allende Prieto, D. An et al., *Astrophys. J. Suppl.* **193**, 29 (2011).
 13. M.A. Strauss, D.H. Weinberg, R.H. Lupton et al., *Astronom. J.* **124**, 1810 (2002).
 14. F.G. Kopylova, A.I. Kopylov, *Asrophys. Bull.* **73**, 267 (2018).
 15. F.G. Kopylova, A.I. Kopylov, *Asrophys. Bull.* **74**, 365 (2019).

16. R.G. Carlberg, H.K.C. Yee, E. Ellingson et al., *Astrophys. J.* **478**, 462 (1997).
17. F.G. Kopylova, A.I. Kopylov, *Asrophys. Bull.* **71**, 257 (2016).
18. C. Tchernin, D. Eckert, S. Ettori et al., *Astronom. and Astrophys.* **595**, A42 (2016).
19. A.I. Kopylov, F.G. Kopylova, *Asrophys. Bull.* **70**, 243 (2015).
20. F.G. Kopylova, A.I. Kopylov, *Asrophys. Bull.* submitted.
21. C.P. Haines, M.J. Pereira, G.P. Smith, et al., *Astrophys. J.* **775**, 126 (2015).
22. F.G. Kopylova, *Asrophys. Bull.* **39**, 1 (2013).
23. S. Barsanti, M.S. Owers, S. Brough et al., *Astrophys. J.* **857**, 72 (2018).
24. K.A. Oman, M.J. Hudson, P.S. Behroozi, *Monthly Notices Roy. Astronom. Soc.* **431**, 2307 (2013).
25. L. Mayer, C. Mastropietro, J. Wadsley, et al., *Monthly Notices Roy. Astronom. Soc.* **369**, 1021 (2006).
26. B.M. Poggianti, I. Smail, A. Dressler, et al., *Astrophys. J.* **518**, 576 (1999).
27. A.R. Wetzel, J.L. Tinker, C. Conroy, & F.C. van den Bosch, *Monthly Notices Roy. Astronom. Soc.* **432**, 336 (2013).
28. C. Haines, A. Finoguenov, G. Smith, et al., *Monthly Notices Roy. Astronom. Soc.* **477**, 4931 (2018).
29. C. Conroy, J.E. Gunn, M. White, *Astrophys. J.* **699**, 486 (2009).
30. A.R. Wetzel, J.L. Tinker and C. Conroy, *Monthly Notices Roy. Astronom. Soc.* **424**, 232 (2012).
31. A.Jr. Oemler, A. Dressler, M.G. Gladders et al., *Astrophys. J.* **844**, 45 (2017).
32. F.G. Kopylova, A.I. Kopylov, *Asrophys. Bull.* **74**, 365 (2020).
33. B. M. Poggianti, R. Calvi, D. Bindoni et al., in the proceedings of the IAU, IAU Symposium, V. 295, 151 (2013).
34. M. Cebrián, I. Trujillo, *Monthly Notices Roy. Astronom. Soc.* **444**, 682 (2014).
35. S. Adhikari, N. Dalal, R. T. Chamberlain, *JCAP* **11**, 19 (2014).
36. J. Matharu, A. Muzzin, G. B. Brammer et al., *Monthly Notices Roy. Astronom. Soc.* **484**, 595 (2019).
37. A. Hamabata, T. Oogi, M. Oguri et al., *Monthly Notices Roy. Astronom. Soc.* **488**, 4117 (2019).
38. F. Pranger, I. Trujillo, L.S. Kelvin, M. Cebrián *Monthly Notices Roy. Astronom. Soc.* **467**, 2127 (2017).

Table 1. Dynamical characteristics of A 2142

Cluster	σ	R_c	R_{200}	R_{sp}	N_z	z_h	M_{200}	$L_{0.1-2.4keV}$
	km c^{-1}	Mpc	Mpc	Mpc			$10^{14} M_\odot$	$10^{44} \text{ erg s}^{-1}$
(1)	(2)	(3)	(4)	(5)	(6)	(7)	(8)	(9)
A 2142	963 ± 70	1.52	2.28	4.12	191	0.090135	14.82 ± 3.23	10.58

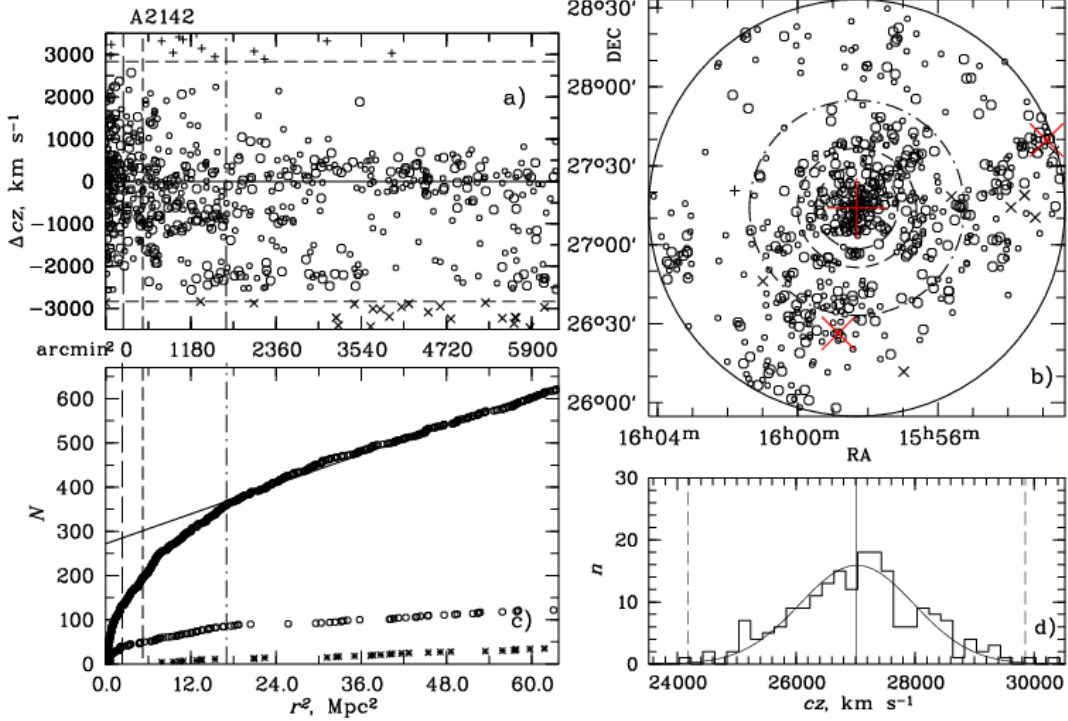


Figure 1. Distribution of galaxies in the cluster A 2142: (a) deviation of the radial velocities of galaxies from the average radial velocity of the cluster determined from the galaxies within the radius R_{200} . The horizontal dashed lines correspond to the deviations $\pm 2.7\sigma$, the vertical lines mark the radii R_{200} (short dashes), R_c (long dashes), R_{sp} (dash-dotted). Larger circles indicate galaxies brighter than $M_K^* + 1 = -24^m$, the plus marks are for background galaxies, and the crosses are foreground galaxies. b) The distribution of the galaxies shown in panel (a) in the sky in equatorial coordinate (the notation is the same). The areas with the radii R_c , R_{200} and R_{sp} are marked with the circles. The research area is limited by a circle with a radius of $3.5R_{200}$ (the solid line). The large plus and crosses indicate the center of the cluster (the brightest galaxy BCG1 with $M_r < -23.^m82$), and two other brightest galaxies (BCG2 with $M_r < -23.^m49$, BCG3 c $M_r < -23.^m27$). (c) The integral distribution of the total number of galaxies (the upper curve) depending on the square of the distance from the center of the A2142. The lower curve corresponds to the early-type RS galaxies ($-0.075 < (g-r) < 0.075$) brighter than $M_r < -20.^m3$. The circles correspond to the galaxies indicated by the circles in panel (a), the asterisks correspond to the background galaxies. (d) The distribution by radial velocities of all the galaxies within the radius R_{200} (the solid line for the cluster members shows the Gaussian corresponding to the radial velocity dispersion of the cluster). The solid vertical line indicates the average radial velocity of the cluster, the dashed lines correspond to the deviations $\pm 2.7\sigma$.

Table 2. A 2142: early-type galaxies on the RS and their properties along the radius

properties	0–0.25 R_{200}	0–1 R_{200}	1–2 R_{200}	2–3 R_{200}	0–1 R_{sp}	1 R_{sp} –3 R_{200}	field
(1)	(2)	(3)	(4)	(5)	(6)	(7)	(8)
$frac_{E1}$	0.51 ± 0.14	0.50 ± 0.06	0.35 ± 0.05	0.27 ± 0.05	0.44 ± 0.04	0.26 ± 0.05	0.27 ± 0.03
$frac_{E2}$	0.78 ± 0.19	0.61 ± 0.07	0.36 ± 0.05	0.29 ± 0.06	0.51 ± 0.05	0.28 ± 0.05	0.30 ± 0.04
Age, Gyr	9.48 ± 0.20	9.38 ± 0.07	9.32 ± 0.09	9.60 ± 0.16	9.35 ± 0.06	9.60 ± 0.14	9.94 ± 0.11
M_r	-20.76 ± 0.10	-20.79 ± 0.04	-20.82 ± 0.04	-20.78 ± 0.09	-20.81 ± 0.03	-20.78 ± 0.08	-20.71 ± 0.03
$\log(Z/Z_{\odot})$	-0.26 ± 0.02	-0.24 ± 0.01	-0.28 ± 0.01	-0.31 ± 0.01	-0.26 ± 0.01	-0.31 ± 0.01	-0.25 ± 0.02
$(g-r)$	0.96 ± 0.01	0.94 ± 0.01	0.92 ± 0.01	0.92 ± 0.01	0.93 ± 0.01	0.92 ± 0.01	0.92 ± 0.01
$R_e, \text{ kpc}$	2.73 ± 0.40	2.84 ± 0.14	3.03 ± 0.17	2.88 ± 0.25	2.92 ± 0.11	2.84 ± 0.23	2.58 ± 0.12

Table 3. A 2142: fraction of galaxies with the quenched star formation along the radius

fraction	0–0.25 R_{200}	0–1 R_{200}	1–2 R_{200}	2–3 R_{200}	0–1 R_{sp}	1 R_{sp} –3 R_{200}	field
(1)	(2)	(3)	(4)	(5)	(6)	(7)	(8)
$frac_{q1}$	0.92 ± 0.22	0.85 ± 0.09	0.65 ± 0.08	0.63 ± 0.09	0.78 ± 0.06	0.60 ± 0.08	0.58 ± 0.10
$frac_{q2}$	0.30 ± 0.10	0.42 ± 0.06	0.39 ± 0.06	0.32 ± 0.06	0.42 ± 0.04	0.30 ± 0.05	0.31 ± 0.09

Table 4. A 2142: parameters of galaxies with the quenched star formation along the radius ($\log M^*/M_{\odot} = [10.5, 11.0]$)

properties	0–0.25 R_{200}	0–1 R_{200}	1–2 R_{200}	2–3 R_{200}	0–1 R_{sp}	1 R_{sp} –3 R_{200}	field
(1)	(2)	(3)	(4)	(5)	(6)	(7)	(8)
$c(R_{90,r}/R_{50,r})$	2.65 ± 0.01	2.56 ± 0.07	2.53 ± 0.06	2.39 ± 0.07	2.54 ± 0.04	2.39 ± 0.07	2.45 ± 0.03
$frac_{DeV}$	0.78 ± 0.01	0.56 ± 0.08	0.55 ± 0.03	0.36 ± 0.08	0.55 ± 0.04	0.36 ± 0.08	0.41 ± 0.04
$(g-r)$	0.94 ± 0.01	0.89 ± 0.01	0.86 ± 0.01	0.89 ± 0.03	0.88 ± 0.01	0.89 ± 0.03	0.80 ± 0.01
age, Gyr	8.88 ± 0.28	8.66 ± 0.08	8.81 ± 0.14	8.70 ± 0.12	8.74 ± 0.08	8.70 ± 0.12	8.91 ± 0.06
$\log(Z/Z_{\odot})$	-0.28 ± 0.01	-0.31 ± 0.02	-0.32 ± 0.03	-0.23 ± 0.09	-0.32 ± 0.02	-0.23 ± 0.09	-0.08 ± 0.03
$c(R_{90,r}/R_{50,r})$	2.69 ± 0.03	2.95 ± 0.07	2.86 ± 0.04	2.85 ± 0.06	2.90 ± 0.04	2.86 ± 0.05	2.86 ± 0.02
$frac_{DeV}$	0.90 ± 0.04	0.95 ± 0.01	0.94 ± 0.01	0.97 ± 0.01	0.95 ± 0.01	0.97 ± 0.01	0.96 ± 0.01
$(g-r)$	0.94 ± 0.03	0.91 ± 0.01	0.89 ± 0.01	0.90 ± 0.01	0.90 ± 0.01	0.89 ± 0.01	0.85 ± 0.01
age, Gyr	8.87 ± 0.16	8.92 ± 0.05	8.85 ± 0.05	8.90 ± 0.06	8.89 ± 0.04	8.89 ± 0.05	9.02 ± 0.05
$\log(Z/Z_{\odot})$	-0.27 ± 0.04	-0.25 ± 0.02	-0.29 ± 0.01	-0.29 ± 0.02	-0.27 ± 0.01	-0.29 ± 0.02	-0.24 ± 0.02

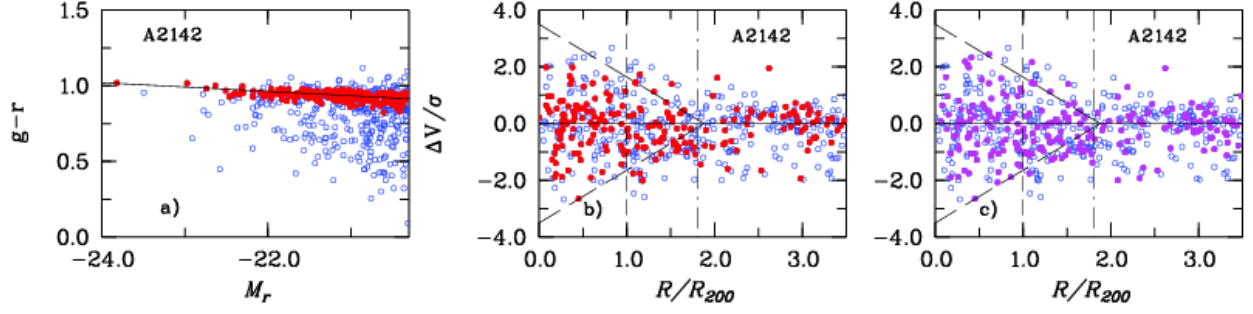


Figure 2. (a) Color–absolute magnitude dependence for the galaxy cluster A 2142. The RS galaxies ($-0.075 < (g - r) < 0.075$) are shown with the solid red circles. (b) and (c) the velocity–radius phase space diagrams, where velocity is the ratio of the radial velocity difference of the galaxies and the average radial velocity of the cluster to the radial velocity dispersion, and R/R_{200} is the distance of the galaxy from the center of the cluster normalized to the radius R_{200} . The dashed and dash-dotted lines show the radii R_{200} and R_{sp} , respectively. The solid red circles in panel (b) are the RS galaxies, as well as in panel (a). In panel (c), the solid magenta circles correspond to the galaxies with the quenched star formation ($-3 \text{ Gyr}^{-1} < \log sSFR < -1.75 \text{ Gyr}^{-1}$). The sloping dashed lines show the model calculations from [23]; they separate the virialized cluster members.

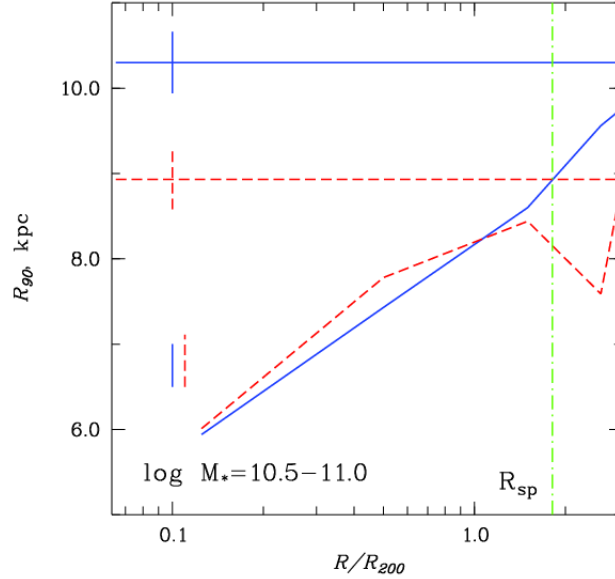


Figure 3. Petrosian average radius $R_{90,r}$ in kiloparsecs of the galaxies with the masses $\log M^*/M_\odot = [10.5, 11.5]$ depending on the normalized radius R/R_{200} . The dashed polygonal red line corresponds to early-type galaxies $fracDeV \geq 0.8$, the solid blue line corresponds to late-type galaxies with $fracDeV < 0.8$. The average values of $R_{90,r}$ obtained from field galaxies of early and late types are marked with horizontal lines of the same type. The vertical short lines show the average errors in the measurements of the radii. The vertical green line corresponds to the cluster radius R_{sp} .